Supporting information for

Iron-based fluorophosphate Na_2FePO_4F as a cathode for aqueous zinc-ion batteries

Deepa Singh,[a] Yang Hu,[b] Sher Singh Meena,[c] Rishikesh Vengarathody,[b] Maximilian Fichtner,[b,d] Prabeer Barpanda[a,b,d]*

[a] *Faraday Materials Laboratory (FaMaL), Materials Research Centre, Indian Institute of Science, Bangalore 560012, India.*
[b] *Helmholtz Institute Ulm (HIU), Electrochemical Energy Storage, Ulm 89081, Germany.*
[c] *Solid State Physics Division, Bhabha Atomic Research Centre, Mumbai, 400085, India.*
[d] *Institute of Nanotechnology, Karlsruhe Institute of Technology (KIT), Karlsruhe 76021, Germany.*

Synthesis Procedure:

Stoichiometric amounts of $NaNO_3$, $Fe^{III}(NO_3)_2.9H_2O$, NaF, and $NH_4H_2(PO_4)_2$ (in a molar ratio of Na: Fe: F = 2:1:1) were dissolved in minimum amount of water with constant magnetic stirring. Citric acid was used as a fuel to ignite the exothermic combustion reaction. This precursor solution was heated to 150 °C to form a gel following dehydration, which spontaneously underwent an exothermic reaction to yield a dark brown powder as an intermediate product known as combustion ash. Following, this combustion ash was mildly ground with an agate mortar and pestle, was pressed into pellets, and was calcined at 600° C for 6 h in a tubular furnace (under steady Ar flow) to obtain the desired product.

The phase purity and crystal structure of the fluorophosphate sample [Na_2FePO_4F] was analyzed by powder X-ray diffraction (XRD) equipped with Cu $K_{\alpha 1}$ (λ = 1.54 Å) radiation source using a PANalytical X'pert pro with a range of 10°-80° and scanning step size of 0.02626° s^{-1}. The sample purity and structural parameters were assessed by Rietveld analysis using the FullProf program. The structural information for Na_2FePO_4F is tabulated in Table S1. The morphology of Na_2FePO_4F was observed using field emission scanning electron microscopy (Carl Zeiss Ultra FE-SEM operated at 5 kV) and transmission electron microscopy (Titan Themis operated at 300 kV).

Material characterization:

Table S1. Structural refinement results and atomic coordinates of orthorhombic Na_2FePO_4F.

Formulae [Molecular weight]	Na_2FePO_4F [215.7943 $gmol^{-1}$]
Crystal System	Orthorhombic
Space group	*Pbcn* (#60)
Unit cell parameters (Å)	*a* = 5.2065(17), *b* = 13.8197(5), *c* = 11.7553(4), *Z* = 8
Unit cell volume ($Å^3$)	845.82(1)
Theoretical density (g cm^{-3})	3.39
Goodness of fit (χ^2)	9.59
Bragg R factor and R_f factor	8.562 and 7.835

atom	**site**	***x***	***y***	***z***	**Occupancy**	**U_{iso}($Å^2$)**	**Site**
Fe	Fe1	0.2403(12)	0.0131(3)	0.3255(4)	1.000	0.320(6)	8d
P	P1	0.2089(13)	0.3874(5)	0.0836(6)	1.000	0.320(6)	8d
Na	Na1	0.2430(3)	0.2498(7)	0.3261(10)	1.000	0.320(6)	8d
Na	Na2	0.2620(3)	0.1261(9)	0.0780(6)	1.000	0.320(6)	8d
F	F1	0.0000	0.1255(8)	0.2500	1.000	0.320(6)	4c
F	F2	0.5000	0.1039(7)	0.2500	1.000	0.320(6)	4c
O	O1	0.2570(14)	0.3875(4)	-0.0428(5)	1.000	0.320(6)	8d
O	O2	0.2775(14)	0.2796(5)	0.1359(5)	1.000	0.320(6)	8d
O	O3	0.084(10)	0.3947(5)	0.1002(5)	1.000	0.320(6)	8d
O	O4	0.3395(10)	0.4673(5)	0.1515(6)	1.000	0.320(6)	8d

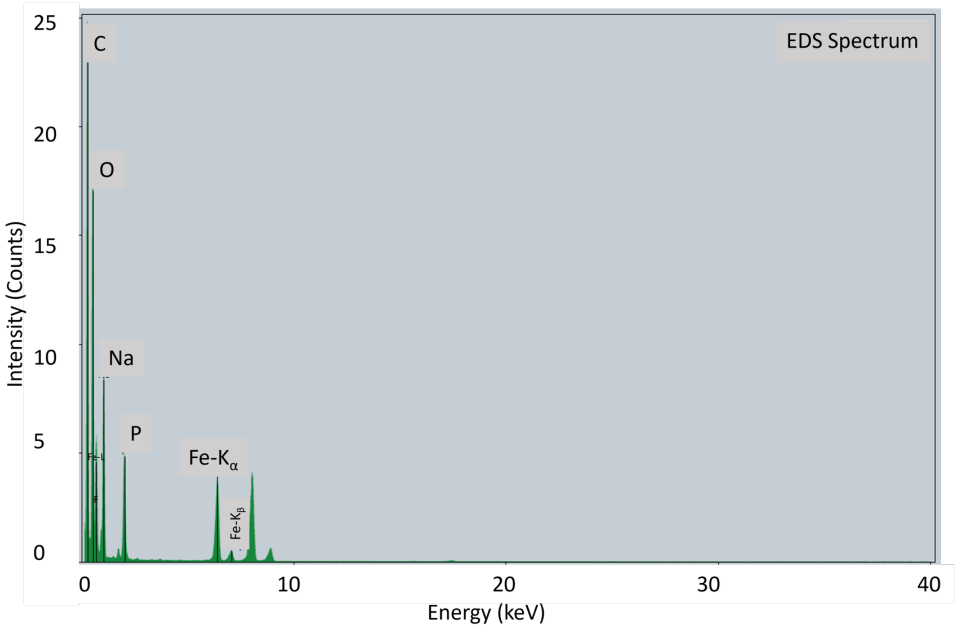

Figure S1. EDS spectrum showing the elemental distribution for Na_2FePO_4F.

Table S2. Quantification of elements though elemental mapping using transmission electron microscopy (TEM) for pristine sample.

Z	Element	Family	Atomic fraction(%)	Atomic error(%)	Mass fraction(%)	Mass error(%)	Fit error(%)
6	C	K	56.35	5.65	41.84	2.64	2.67
8	O	K	22.68	5.04	22.84	4.75	0.24
9	F	K	3.50	0.81	3.74	0.82	6.74
11	Na	K	9.02	1.99	11.62	2.40	0.55
15	P	K	4.52	0.96	7.69	1.53	0.09
26	Fe	K	3.93	0.65	12.28	1.78	0.18

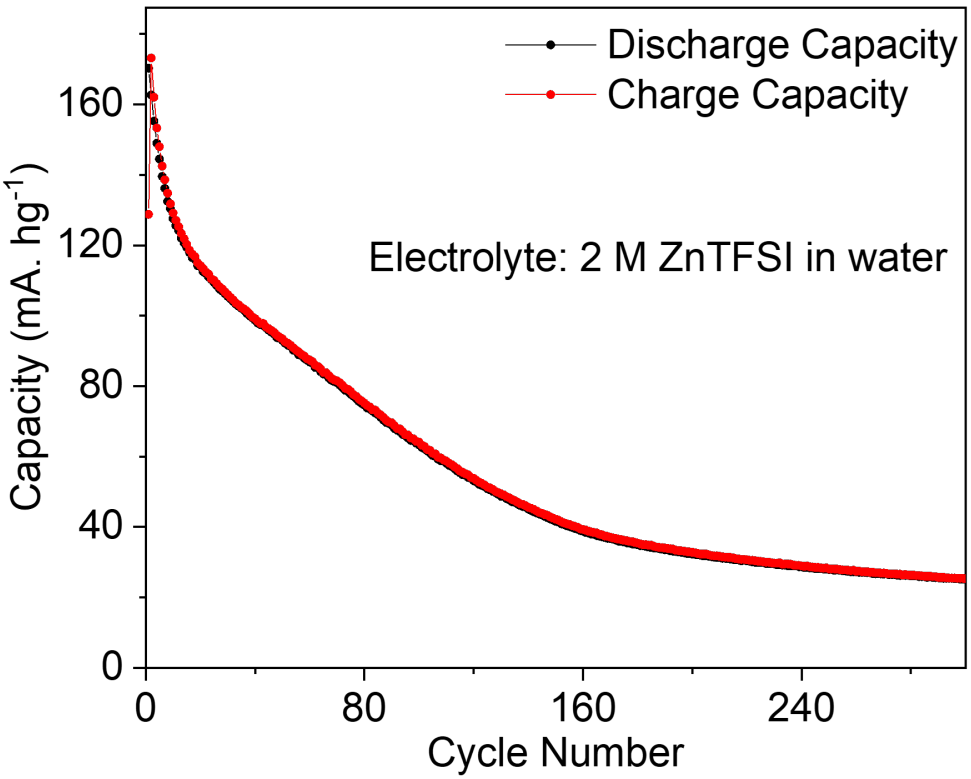

Figure S2. Electrochemical performance of Na_2FePO_4F in 2 M Zn $(TFSI)_2$ electrolyte.

Cell preparation:

Careful preparation and handling of cathode materials are crucial to obtain robust electrochemical cyclability. First, we prepared our electrodes by homogeneously mixing active materials with Super P carbon black and polyvinylidene fluoride (PVDF) binder in a 7:2:1 (w/w) ratio. The slurry was prepared in N-methyl-2-pyrrolidine (NMP) and was hand-coated onto the stainless-steel substrates. After drying them overnight in the vacuum oven, they were further used as cathodes for cell preparation. All the galvanostatic charge-discharge cycling were carried out in swagelok setup using 3 M zinc triflate $[Zn(CF_3SO_3)_2]$ as electrolyte.

Experimental details

1. Mössbauer analysis: Mössbauer spectra (MS) at room temperature were recorded with a conventional spectrometer operated in constant acceleration mode and transmission geometry with Co^{57} source in Rh matrix of 5mCi. The recorded MS were fitted using the WinNormos site fit program.[1] The calibration of the velocity scale was done by using an enriched α-^{57}Fe metal foil. The isomer shift values were relative to the Fe metal foil (δ= 0.0 mm/s). All the values were correlated with the goodness of fit (χ^2) values.

Table S3. Mössbauer analysis results of quadrupole splitting (ΔE_Q), isomer shift (δ), line width (Γ), and relative area (R_A) of Fe sites with their goodness of fit in pristine and (dis)charged Na_2FePO_4F samples. All Mössbauer spectra were recorded at room temperature. (NFPF-P = pristine Na_2FePO_4F, NFPF-1C = Na_2FePO_4F after 1st charge, NFPF-1D = Na_2FePO_4F after 1st discharge).

Sample Comp. (*x*)	**Fe sites**	**Quadrupole splitting (ΔE_Q) mm/s ±0.007**	**Isomer shift (δ) mm/s ±0.005**	**Line width (Γ) mm/s ±0.005**	**Relative Area, R_A (%)**	**Goodness of fit (χ^2)**
NFPF-P	Doublet 1 (Fe^{2+})	2.270	1.234	0.421	87.5	0.96
	Doublet 2 (Fe^{3+})	0.454	0.442	0.500	12.5	
NFPF-1C	Doublet 1 (Fe^{2+})	2.299	1.163	0.322	18.5	1.04
	Doublet 2 (Fe^{3+})	0.560	0.418	0.326	81.5	
NFPF-1D	Doublet 1 (Fe^{2+})	2.342	1.201	0.363	50.4	0.95
	Doublet 2 (Fe^{3+})	0.414	0.425	0.373	49.6	

2. Description of X-ray absorption spectroscopy (XAS): Both XANES and EXAFS showed changes after 1st charge and discharge. We observed in the XANES spectra (in the manuscript) that there is an apparent oxidation state change after 1st cycle, where the Fe(II) got oxidized to

Fe(III) evidenced by the edge shifts toward higher energy values. It was confirmed using the reference of FeO for the reduced state, whereas the reference was Fe_2O_3 for the oxidized state. There is no significant change in pre-edge peak intensity (shown in the inset).

In EXAFS, Fe K-edge XAFS was performed on the pristine electrode (NFPF), the electrode after the first charge (NFPF-1C) and discharge (NFPF-1D) in the fluorescence mode. The obtained spectra were first calibrated and normalized using Athena and Demeter packages.[2] A smooth quadratic spline polynomial was used for background subtraction with R_{bkg} = 0.95 $Å^{-1}$ in the k range 0 ~ 12 Å. The isolated $\chi(k)$ data were k^2-weighted and Fourier transformed after applying a Hanning window function ($dk = 1$) over 2~8(7.5) $Å^{-1}$. A theoretical model was computed using FEFF6 in Atoms[3] based on a structure file of $Na_2Fe(PO_4)F$ (ICSD 194076), generating four single-scattering paths for the nearest four oxygen and two fluorine atoms surrounding the central absorbing Fe atom. Shell fitting was carried out on Artemis package.[4] The amplitude reduction factor S02 was obtained from fitting the Fe foil and was fixed to 0.8. To reduce the number of independent variables which were limited by the high noise ratio, the degeneracy in each path was fixed to the calculated value. Moreover, a fixed ratio x was applied to the variation of all half-path lengths, and the resulting interatomic distance was $R_{path\_i} = R_{reff\_i}$ (calculated) + ΔR_{path_i} (= R_{reff_i} * x). The disorder factor σ^2 was constrained the same for the three nearer atoms (Fe-F1, Fe-O1) and for the three further atoms (Fe-O2, Fe-F2), respectively. Figure S3 shows the EXAFS fitting of NFPF in this work. It is worth noting that the number of independent variables was very limited due to the high noise ratio at high k region, and therefore quite strong constraints were applied. The change in half-path lengths ΔR was treated by applying one variation ratio to the calculated R_{reff} for all paths, as in cubic structure where all lattice change was assumed to be isotropic. Nevertheless, we observed a general decrease of the interatomic distance for all four paths from pristine to charged samples, as shown in Table S4. This was probably associated with desodiation upon charge, which might lead to similar effects on long-range crystallographic structure and on the short-range local structure. The discharged electrode (NFPF-1D) displayed a general increase of R compared with the charged state, which probably resulted from the Zn intercalation that also led to a contraction of local structure. However, after the first discharge, the interatomic distances were all shorter than those obtained from the pristine electrode. It implies that the local environment of Fe was not fully reverted to the pristine state. While the NFPF and NFPF-1D showed some similarity, NFPF-1C exhibited distinct spectra features and notably higher amplitude in $|\chi(R)|$.

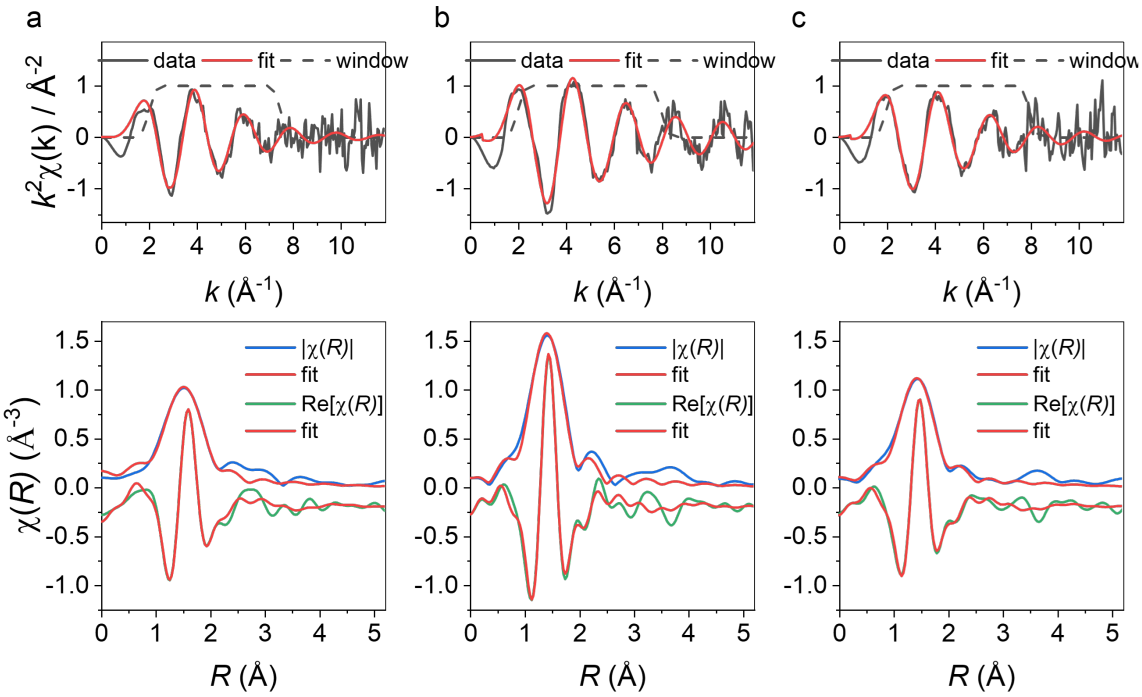

Figure S3. EXAFS fits of (a) pristine NFPF, and the electrode after (b) the first charge (NFPF-1C) and the first discharge (NFPF-1D). Upper graphs are the k^2-weighted χ(k) spectra, lower graphs are the corresponding Fourier transform over the range 2~ 8 Å^{-1} (2~7.5 Å^{-1} for NFPF) after applying a hanning window function (*dk* = 1, black dashed lines). |χ(R)| and Re[χ(R)] display the magnitude and the real part of Fourier transformed spectra, respectively. All red lines represent the fitting results.

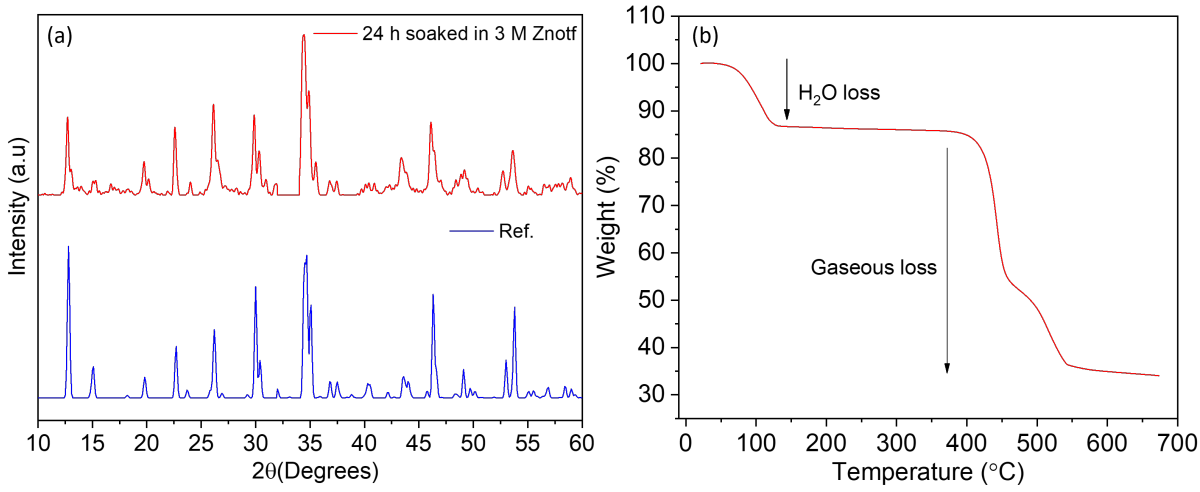

Figure S4. (a) XRD and (b) TGA profiles for the Na_2FePO_4F material soaked in 3 M $Zn(Otf)_2$ for 24 h. The XRD and TGA of the electrode material was conducted after immersing the electrode inside a mildly acidic solution for 24 h and recuperating the electrode after 1 day.

Table S4. EXAFS fits of the Fe *K*-edge spectra from the NFPF electrodes using four single-scattering paths (Fe-F1, Fe-O1, Fe-O2, Fe-F2). *r*-factor indicates the goodness-of-fit, E_0 denote the threshold energy, S02 is the amplitude reduction factor. For each individual path, *R*, N and σ^2 represent the average interatomic distance (half-path length), the number of atoms, and the mean square relative displacement in *R* (disorder).

Sample	Paths	S02 *	N +	E_0(ev)	*R*(Å) ‡	σ^2(Å^2) †	*r*-factor
NFPF	Fe-F1	0.8	1	1(3)	2.03(6)	0.008(6)	0.002
	Fe-O1	0.8	2		2.05(6)		
	Fe-O2	0.8	2		2.17(7)	0.02(2)	
	Fe-F2	0.8	1		2.17(6)		
NFPF-1C	Fe-F1	0.8	1	1(1)	1.91(2)	0.002(2)	0.004
	Fe-O1	0.8	2		1.93(2)		
	Fe-O2	0.8	2		2.04(2)	0.002(1)	
	Fe-F2	0.8	1		2.04(2)		
NFPF-1D	Fe-F1	0.8	1	1(1)	1.96(2)	0.007(2)	0.003
	Fe-O1	0.8	2		1.98(2)		
	Fe-O2	0.8	2		2.09(2)	0.03(1)	
	Fe-F2	0.8	1		2.09(2)		

* S02 obtained from fitting the reference Fe foil

+ The number of atoms was fixed according to the structure model

‡ The same ratio of variation was assigned to all path-lengths as $\Delta R = R_{eff}$ * alpha (the ratio)

† The disorder factor σ2 was constrained the same for the three nearer atoms (Fe-F1, Fe-O1) and for the three further atoms (Fe-O2, Fe-F2), respectively.

3. Description of ex-situ SEM: The pristine Na_2FePO_4F has an agglomerated morphology seen in both the 2nd charge and 2nd discharge samples (Figure S5 a, b). After the electrode was cycled 5 times, the morphology showed a remarkable transformation from agglomerated to flaky nanoparticles (Figure S5 c, d) (marked by yellow dotted circles). This morphology alteration suggests that when the electrode was cycled for 10 cycles, there is a formation of

flake kind of particles at the end of discharge. It belongs to ZHT (Figure S5 e, f) (marked by yellow dotted square) that falls in the category of zinc hydroxy triflate (LDH) byproduct formation leading to an irreversible (de)insertion in the following cycles, could be due to pH alteration as there is an involvement of H^+ as well. Concerning Zn, while there is minimal change in the positions of XRD peaks, an apparent change was noticed in the peak intensities at 2θ values of 36.29˚ and 38.9˚ (Figure S6 a). The intensity of the peak at 36.29˚increases after 10^{th} cycle, whereas the reverse was observed for the peak at 38.9˚. It suggests flake deposition of Zn further happening along the plane corresponding to 36.29˚ (Figure S6 b, c).

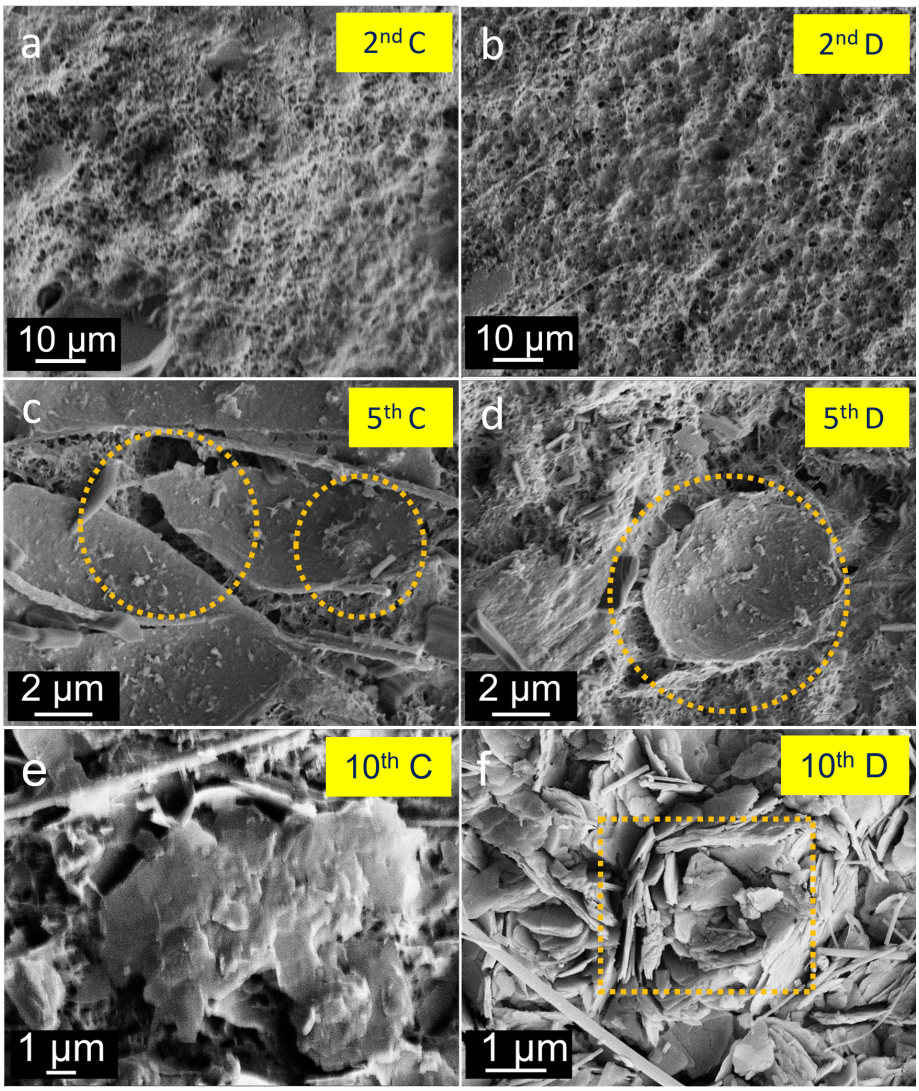

Figure S5. Ex-situ SEM images for Na_2FePO_4F cathode at the 2^{nd}, 5^{th} and 10^{th} cycle which showed an apparent change in the morphology. Initially shows porous agglomerates (a, b), the transforms to flakes in 5^{th} (dis)charge (c, d) (shown by yellow dotted circles), and then the complete coverage of the surface by ZHT flakes (e, f) in 10^{th} dis(charge) (shown by yellow dotted square) with the small glass fiber separator presence (nanowires).

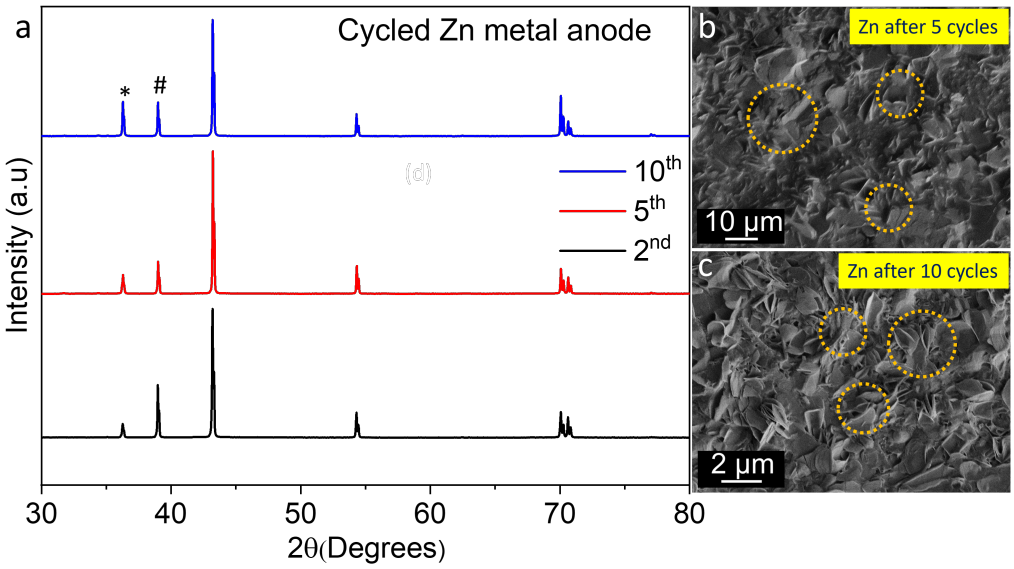

Figure S6. (a) Ex-situ XRD for cycled Zn metal anode at the 2nd, 5th and 10th cycle showing an intensity change marked by (* and #). Ex situ SEM images for cycled Zn metal anode illustrating the evolution of morphology after (b) 5th cycle and (c) 10th cycle where the surface was covered by nanoflakes (shown by dotted yellow circles).

4. Description of XPS measurements: Ex situ XPS measurements were conducted for Na_2FePO_4F at different DOD and SOC (2nd, 5th, and 10th cycle). Initially, Na 1*s* showed a binding energy change after the 5th charge and again after the 10th discharge. The intensity value reverted to normal at the end of both discharge suggesting a possibility of Na co-insertion/deinsertion happening along with Zn (Figure S7 a). There was no apparent change in Fe 2*p* peak except for the binding energy shift to higher or lower values while charging and discharging, respectively. Changes in the O 1*s* and F 1*s* binding energy values at the end of charge and discharge suggest the formation of a few oxygen-related (O-H/O-Zn) and fluorinated species (Zn-F/C-F) at the end of discharge, which is irreversible even after the charge (Figure S7 b, c). In the pristine state, S *2p* peak belongs to SO_3^{2-} species corresponding to the triflate electrolyte. In the dis(charge) state, it showed an appearance of the S 2*p* peak which is related to the formation of fluorinated zinc hydroxy triflate by-product. Overall, the presence of S 2*p* along with O 1*s* further confirmed the formation of LDH.

Additionally, the change in the Zn 2*p* spectra confirmed the Zn (de)insertion. It almost remains constant at the end of charge/discharge. Hence, the amount of inserted Zn does not deintercalate entirely after the charging state, which could also be a cause for capacity degradation (Figure S8 a, b). Overall, it suggests the deposition of zinc hydroxy fluorinated species over the surface is not very reversible to dissolve back in subsequent cycles. It could be the main reason behind capacity degradation even at lower current rates.

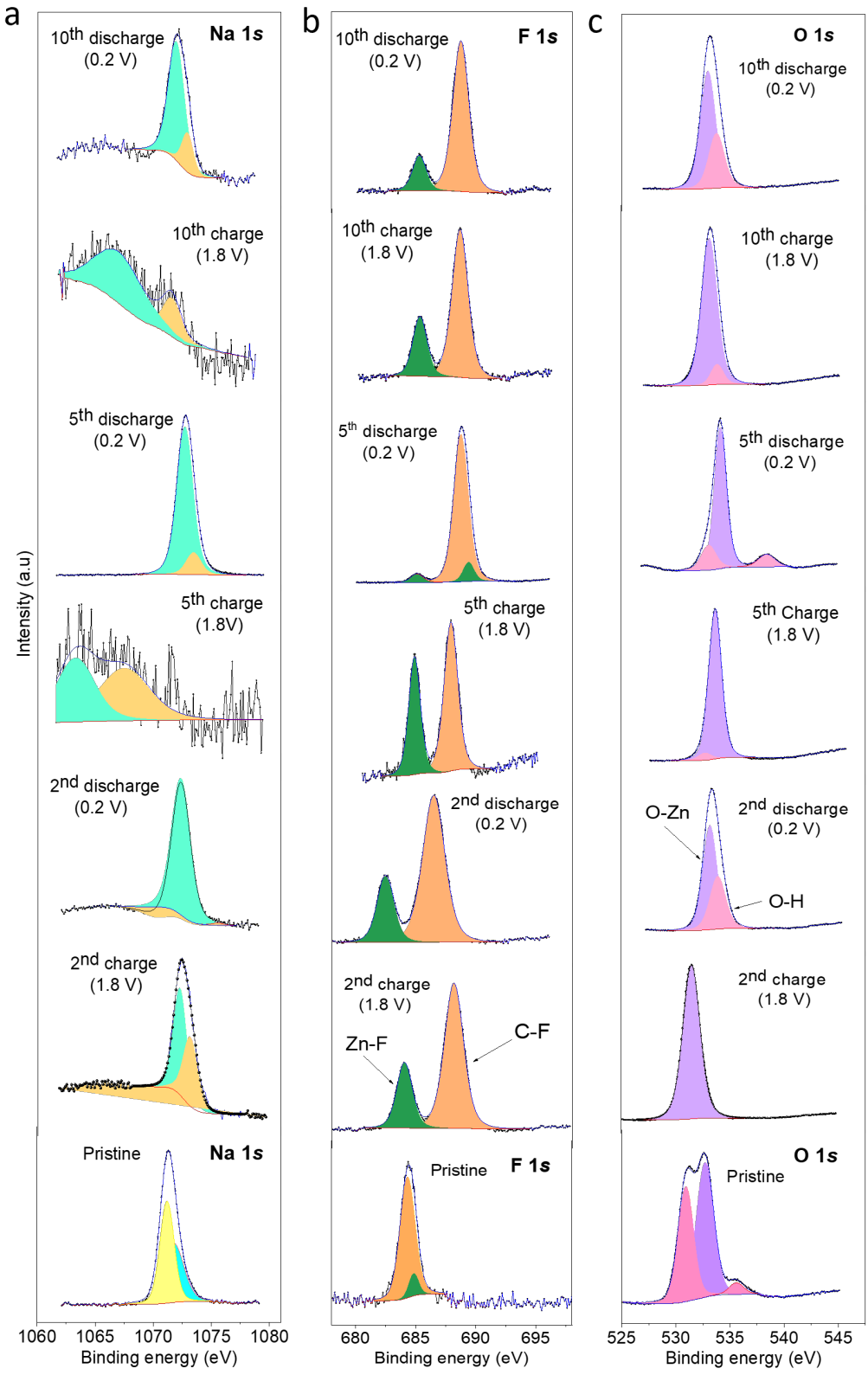

Figure S7. Comparative XPS spectra showing the (a) Na 1*s*, (b) F 1*s*, and (c) O 1*s* peak for pristine NFPF and at the end of 2nd, 5th and 10th charge/discharge. F 1*s* shows the formation of Zn-F/C-F bonded species corresponding to ZHT. O 1*s* shows the presence of O-H/O-Zn bonded species.

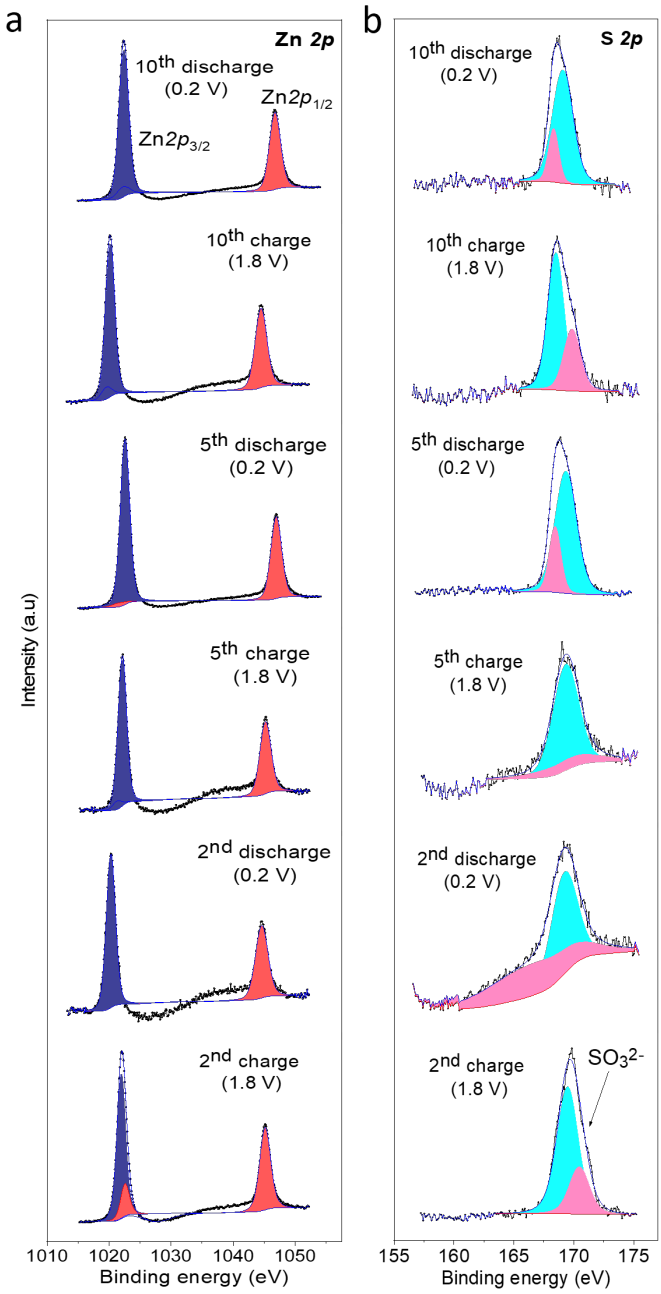

Figure S8. Comparative XPS spectra showing the (a) Zn *2p*, *and* (b) S *2p* peak of NFPF at the end of 2nd, 5th and 10th charge/discharge. Zn 2*p* showed that there is Zn presence on the surface even at the charged step corresponding to ZHT, and S 2*p* peak confirms the SO_3^{2-} presence in ZHT.

For the Zn (anode) side, there is an evident deposition of fluorinated oxide species (C-F/Zn-F/O-H/O-Zn), confirmed by the O 1*s* and F 1*s* spectra. It showed an emergence at the end of the 5th and 10th discharge. A clear F 1*s* peak appeared at the end of both the cycled Zn electrodes. On the Zn side, only a minute amount of S is present, but there is a presence of

fluorine and oxygen as confirmed by O 1*s*, O 2*s*, and F 1*s* spectra after the 5th and 10th discharges (Figure S9a-h).

From XPS data, we could interpret that a pure Zn intercalation does not occur in the system. At the same time, there is some Na content that is also getting changed (de)insertion) after the end of discharge. So, a co-intercalation of Na^{+}/Zn^{2+} is also possible along with the deposition of ZHT, its dissolution is almost irreversible. However, we believe the Na content is not changing as much, and it's almost equal to the deintercalated form of Na_2FePO_4F, which confirms that we can take out the possibility of Na^{+}/Zn^{2+} co-intercalation. However, the process can be more like Co-intercalation of H^{+}/Zn^{2+}

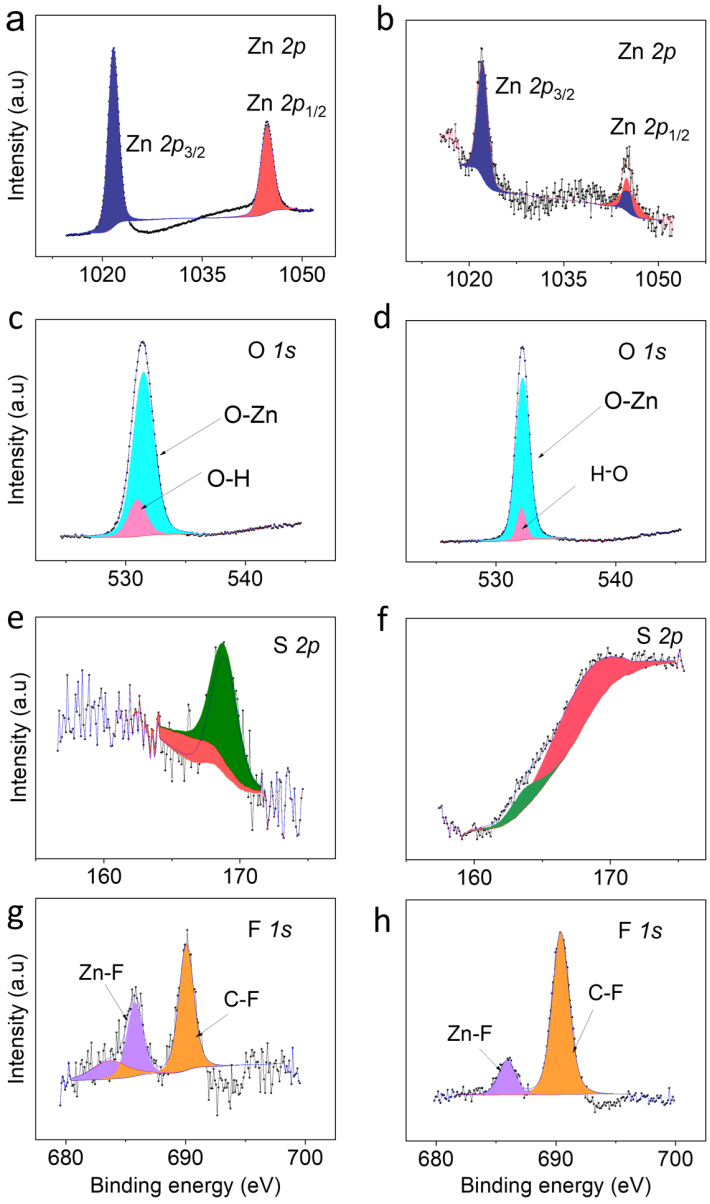

Figure S9. Comparative XPS spectra for cycled Zn metal after (left) 5th discharge and (right) 10th discharge. (a, b) Zn 2*p*, (c, d) O 1*s*, (e, f) S 2*p*, (g, h) F 1*s*.

5. Description of SEM-EDS: Both the cycled cathode and Zn anode showed the presence of by-product formation (ZHT) as shown in Figure S10 a-d and Figure S11 a-b.

Also, the structure is not relatively stable after some cycles for feasible Zn (de)intercalation. The intercalation sites are getting partially occupied by unrecoverable Zn sitting at those sites, leading to the observed capacity degradation.

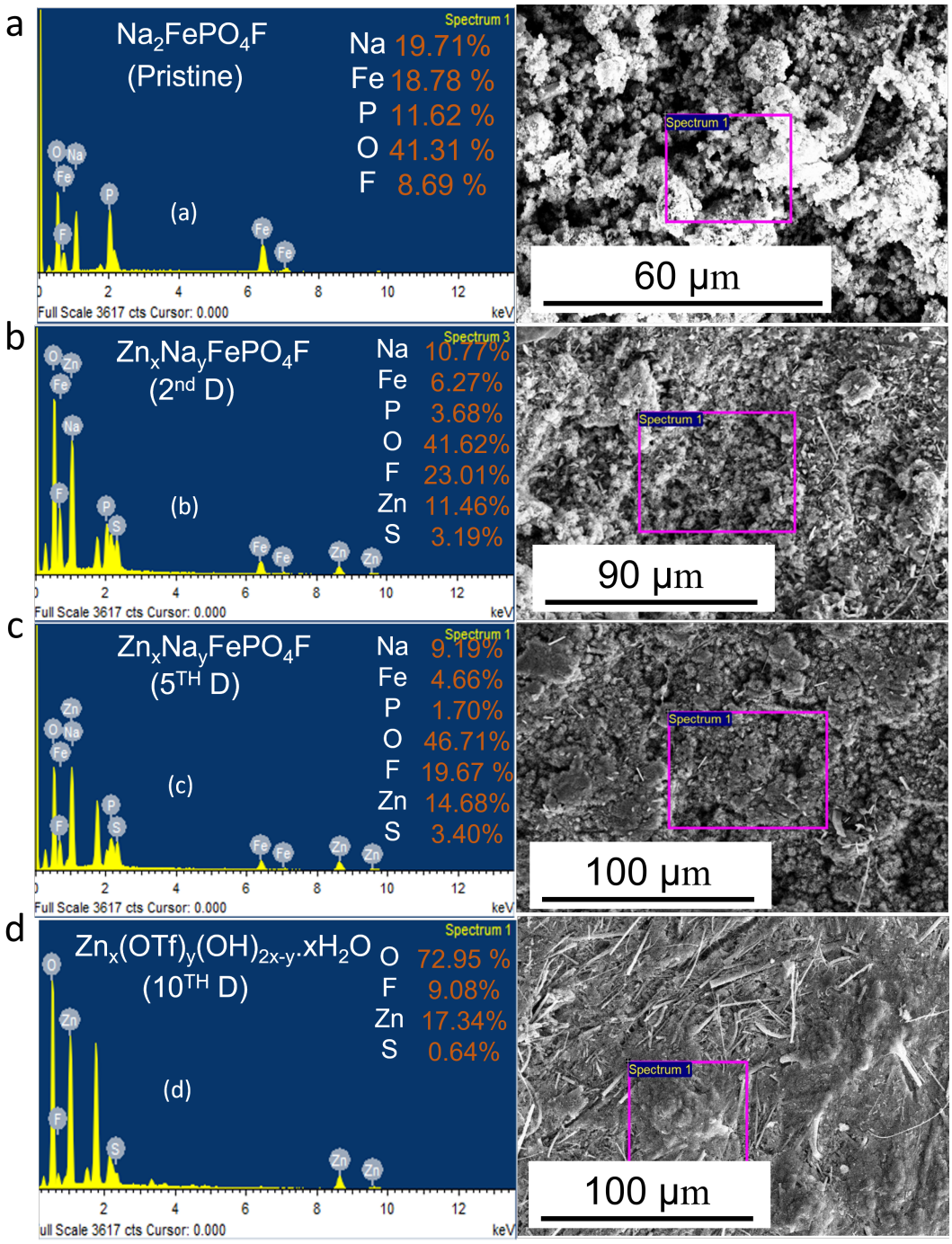

Figure S10. SEM-EDS analysis for (a) pristine NFPF, and cycled cathodes after (b) 2^{nd} discharge, (c) 5^{th} discharge, and (d) 10^{th} discharge.

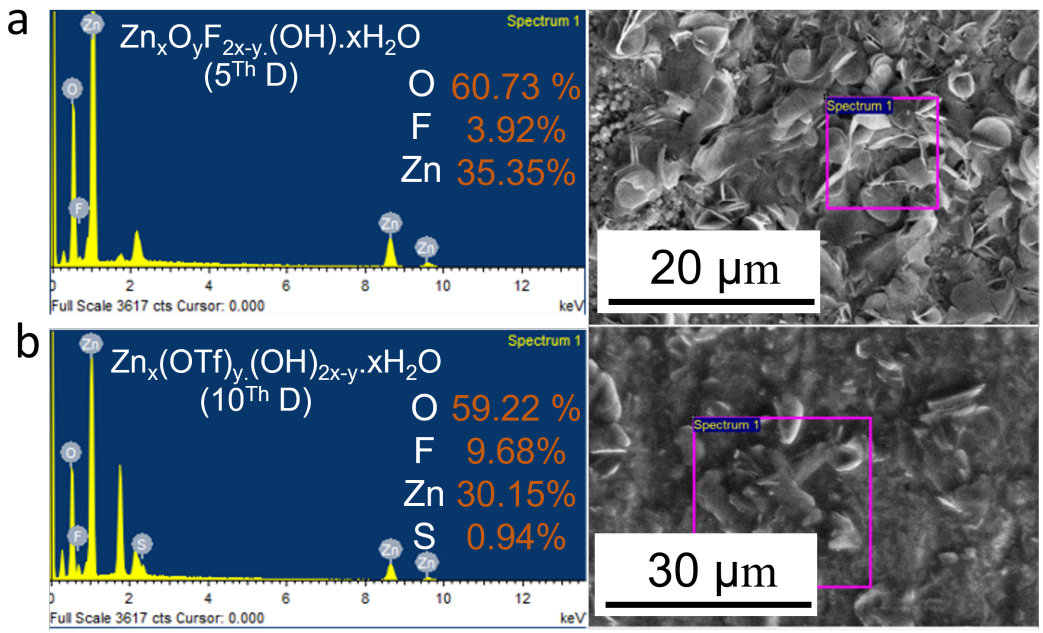

Figure S11. SEM-EDS analysis for cycled Zn anode after (a) 5th discharge, and (b) 10th discharge.

6. Description of FTIR analysis: The FTIR spectra of both the discharged cathode and Zn anode (after the 10th cycle) show the presence of a -OH stretching peak around 3500 cm^{-1} (Figure S12). It confirms the presence of -OH species at the end of product deposition. Though there is a slight difference in peak broadness which was broader in the case of cycled Zn compared to the cathode area, it could be because -OH formation is not quite prominent on the cathode surface.

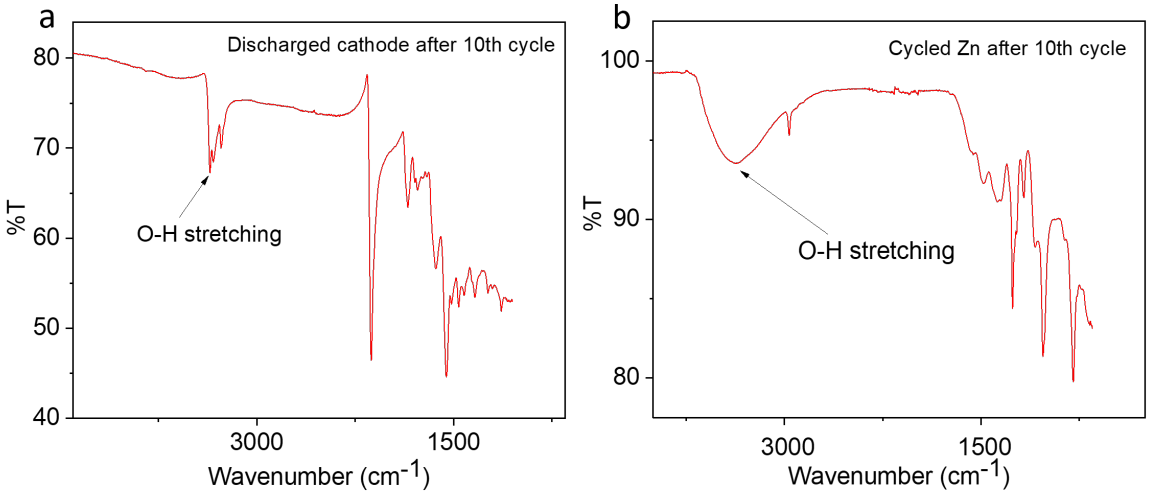

Figure S12. FTIR analysis for discharged cathode(a), and for cycled Zn anode(b) after 10th discharge.

7. Description of structure: Overall, if we want to describe a proper mechanism through crystal structure description, it suggests that in the beginning, we have orthorhombic Na_2FePO_4F. After first charging to 1.8 V, one Na from the lowest energy site came out, and the structure became desodiated with the chemical formulae of $NaFePO_4F$. Further, when the system was discharged to 0.2 V, there was a progressive intercalation of Zn on the vacant sites while charging leading to a chemical formula of $Zn_xNa_yFePO_4F$ (Figure S13).

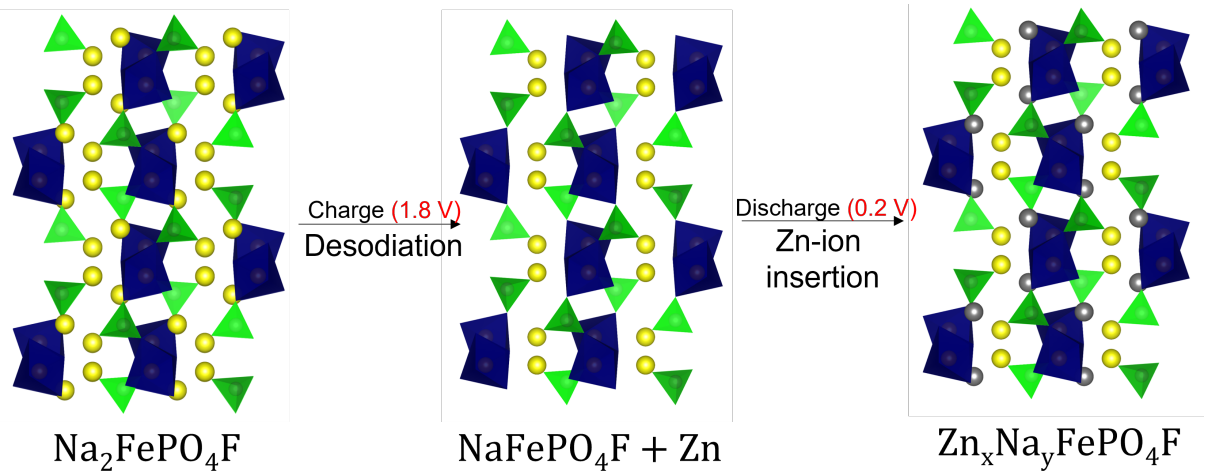

Figure S13. *Crystal structure* changes for Na_2FePO_4F after charging (desodiation) and discharging (Zn-ion insertion).

References:

1. WissEl, Data Evaluation Software-WissEl, Wissenschaftliche Elektronik Gmb, http://www.wisselgmbh.de/index.php?option=com_content&task=view&id=55&Itemid=116.
2. B. Ravel and M. Newville, *J Synchrotron Radiat*, 2005, **12**, 537-541.
3. M. Newville, *J Synchrotron Radiat*, 2001, **8**, 96-100.
4. B. Ravel, *Journal of Synchrotron Radiation*, 2001, **8**, 314-316.